THE JOURNAL OF BIOLOGICAL CHEMISTRY
Vol. 277, No. 47, Issue of November 22, pp. 45518–45528, 2002
Printed in U.S.A.

An Iron-responsive Element Type II in the 5′-Untranslated Region of the Alzheimer's Amyloid Precursor Protein Transcript*

Received for publication, July 24, 2002, and in revised form, August 23, 2002
Published, JBC Papers in Press, August 26, 2002, DOI 10.1074/jbc.M207435200

Jack T. Rogers‡§¶, Jeffrey D. Randall§‖, Catherine M. Cahill, Paul S. Eder‡‡, Xudong Huang‡‖‖, Hiromi Gunshin‡, Lorene Leiter‖, Jay McPhee‖, Satinder S. Sarang‖, Tada Utsuki‡‡, Nigel H. Greig‡‡, Debomoy K. Lahiri§§, Rudolph E. Tanzi‡, Ashley I. Bush‡, Tony Giordano‡‡, and Steve R. Gullans‖**

*From the ‡Genetics and Aging Research Unit, Department of Psychiatry and **Diabetes Unit, Massachusetts General Hospital and ‖Center for Neurologic Diseases and Department of Medicine, Brigham and Women's Hospital, Harvard Medical School, Charlestown, Massachusetts 02129-4404, ‡‡Message Pharmaceuticals, Malvern, Pennsylvania 19355, and §§Department of Psychiatry, Indiana University School of Medicine, Indianapolis, Indiana 46202*

Iron-responsive elements (IREs) are the RNA stem loops that control cellular iron homeostasis by regulating ferritin translation and transferrin receptor mRNA stability. We mapped a novel iron-responsive element (IRE-Type II) within the 5′-untranslated region (5′-UTR) of the Alzheimer's amyloid precursor protein (APP) transcript (+51 to +94 from the 5′-cap site). The APP mRNA IRE is located immediately upstream of an interleukin-1 responsive acute box domain (+101 to +146). APP 5′-UTR conferred translation was selectively downregulated in response to intracellular iron chelation using three separate reporter assays (chloramphenicol acetyltransferase, luciferase, and red fluorescent protein reflecting an inhibition of APP holoprotein translation in response to iron chelation. Iron influx reversed this inhibition. As an internal control to ensure specificity, a viral internal ribosome entry sequence was unresponsive to intracellular iron chelation with desferrioxamine. Using RNA mobility shift assays, the APP 5′-UTRs, encompassing the IRE, bind specifically to recombinant iron-regulatory proteins (IRP) and to IRP from neuroblastoma cell lysates. IRP binding to the APP 5′-UTR is reduced after treatment of cells with desferrioxamine and increased after interleukin-1 stimulation. IRP binding is abrogated when APP cRNA probe is mutated in the core IRE domain (Δ4 bases:Δ83AGAG86). Iron regulation of APP mRNA through the APP 5′-UTR points to a role for iron in the metabolism of APP and confirms that this RNA structure can be a target for the selection of small molecule drugs, such as desferrioxamine (Fe chelator) and clioquinol (Fe, Cu, and Zn chelator), which reduce Aβ peptide burden during Alzheimer's disease.

The amyloid precursor protein (APP)[1] is cleaved into the 40–42-amino acid Aβ peptides that constitute the main component of the neurotoxic amyloid plaques formed during the progression of Alzheimer's disease (AD) and Down's syndrome (1, 2). In healthy individuals, APP holoprotein is expressed ubiquitously as a protein resembling a type I transmembrane receptor and metal-binding protein (3–6). Secreted APP (APP(s)) is neurotrophic (7).

There are now several reports supporting an important role for translational regulatory mechanisms to control APP synthesis and probably Aβ peptide secretion in biologically relevant circumstances (8). First, interleukin-1 (IL-1), the first cytokine released during the acute phase response, significantly increases APP protein synthesis in astrocytes without altering APP mRNA levels (9). IL-1 acts by regulating APP and ferritin genes at the level of message translation (9). Second, reversible ischemic assault significantly increases APP levels without any alteration in the steady-state levels of APP mRNA in rabbit spinal cord neurons (10). Third, APP mRNA 3′-UTR sequences located between alternative poly(A) selection sites maintain efficient translation of microinjected APP in *Xenopus* oocytes and in Chinese hamster ovary transfectants (11).

Iron-responsive elements (IREs) are RNA stem loops that post-transcriptionally control the balance of cellular iron storage and transport (12). IREs mediate iron-induced up-regulation of the L- and H-subunits of the universal iron storage protein ferritin (13–16). Translation of the L and H ferritin mRNAs (L- and H-mRNAs) is repressed by the binding of iron-regulatory proteins (IRPs) to the 5′-cap-specific IRE stem loops (17, 18). IRP-1 (90 kDa) and IRP-2 (105 kDa) interact with IREs to suppress ferritin translation (19, 20). Iron influx releases IRP-induced translational repression of ferritin by lowering the binding affinity of IRP-1 to the IRE and enhancing the degradation of IRP-2 (18, 21, 22).

The recent finding that IRP-2 knock-out mice develop a motor disorder with ataxia, bradykinesia, and tremor (18) supports a possible role for the disruption of brain iron levels and compartmentalization in the etiology of neurodegenerative dis-

* This work was supported by Grant 210802 from the Institute for the Study of Aging (ISOA) (to J. T. R.), Grant IIRG-02-3524 from the Alzheimer's Association, an American Federation for Aging Research/ISOA (AFAR/ISOA) grant in drug discovery, and by National Institutes of Health Grant R03 (to J. T. R.). The costs of publication of this article were defrayed in part by the payment of page charges. This article must therefore be hereby marked "*advertisement*" in accordance with 18 U.S.C. Section 1734 solely to indicate this fact.

§ Contributed equally.

¶ To whom correspondence should be addressed: Genetics and Aging Research Unit, Department of Psychiatry-Neuroscience, Mass General (East), Harvard Medical School, Bldg. 114, 3850 16th St., Charlestown, MA 02129-4404. Tel.: 617-726-8838; Fax: 617-726-5677.

‖‖ Supported by K Award 5K01MH02001.

[1] The abbreviations used are: APP, amyloid precursor protein; AD, Alzheimer's disease; APP(s), secreted APP; IL, interleukin; UTR, untranslated region; IRE, iron-responsive elements; IRP, iron-regulatory proteins; FAC, ferric ammonium citrate; CAT, chloramphenicol acetyltransferase; nt, nucleotide; IRES, internal ribosome entry site element; RFP, red fluorescent protein; REMSA, RNA electrophoretic mobility shift assay; GFP, green fluorescent protein; RPC, RNA-protein complexes; Df, desferrioxamine; DFO, desferrioxamine; APLP-1, amyloid precursor-like protein 1.

eases. Mutations to the hemochromatosis gene have been linked to the age of onset of AD (23). AD patients display enhanced levels of the metal in the cortex regions of the brain (24). Metals are present in the brains of AD patients at higher levels than age-matched control subjects (25, 26) leading to an altered pattern of IRE-IRP binding (27). Also the iron storage protein ferritin is present in neuritic amyloid plaques (28). Intracellular iron levels modulate the cleavage of APP and cause a higher secretion of APP ectodomain (APP(s)) into the conditioned medium of Chinese hamster ovary cells (29). Iron may modulate the levels of cellular APP associated with protein processing by α-secretase, a metalloprotease that is a member of the ADAM family of metalloproteases (30, 31).

In this report we extend our previous observations that characterized how IL-1 controls APP translation to show the presence of a novel and functional iron-regulatory element within the 5′-UTR of APP mRNA (+51 to +94 from the 5′-cap site). This IRE, which we name IRE-Type II, is located immediately upstream of the IL-1 responsive acute box domain in the 5′-UTR of APP mRNA (+101 to +146), similar to the ferritin L- and H-mRNAs. The APP 5′-UTR was selectively responsive to intracellular iron levels in a pattern that reflects iron-dependent regulation of intracellular APP synthesis. To assess specificity to iron levels, two separate viral RNA sequences were shown to be unresponsive to intracellular iron chelation with desferrioxamine. Finally APP mRNAs specifically bound iron-regulatory proteins (IRP-1 and/or IRP-2) in the 5′-UTR whereas IRP binding no longer occurred when cRNA probes were mutated in the core IRE homology domain in the APP 5′-UTR translational control element.

EXPERIMENTAL PROCEDURES

APP Protein Synthesis

Neuroblastoma cells (SHSY-5Y) were exposed to 50 and 250 μM desferrioxamine and iron supplement as 100 and 500 μM ferric ammonium citrate (FAC) for 24 and 48 h. Metabolic labeling of neuroblastoma cells was performed for 30 min using 10 μCi/ml [^{35}S]methionine in methionine-free medium (Invitrogen), and pulse-labeled APP was immunoprecipitated from lysates as described previously (9). Western blotting was performed using a Bio-Rad apparatus to electrophorese the proteins (20-μg uniform loading), which were run at 100 V and transferred at 200 V according to manufacturer's instructions. Prior to loading, protein content was determined by protein BCA assays (Pierce) and standardized to allow equal loading of each lane. APP(s)-specific R1753 antibody was a gift from Dr. Dennis Selkoe. Used at a 1:1,500 dilution, R1753 recognizes amino acids 596–611 in APP. Immunoprecipitations were performed using the C8 antibody, which recognizes APP amino acids 676–695. Blots were quantitated using NIH Image.

APP mRNA Levels

Northern blots were performed on iron-treated and desferrioxamine-treated neuroblastoma cells (SHSY-5Y and SKNSH) as described (9). A 3-kb *Sma*I fragment of APP cDNA was random prime-labeled and hybridized to Northern blots loaded with 10 μg of total RNA per well. Random prime-labeled ferritin cDNA and glyceraldehyde-3-phosphate dehydrogenase cDNAs were used to standardize the northern blots for differences in sample loading.

Construct Preparation

The pSV2(APP)CAT construct encoded the 90-nt *Sma*I-*Nru*I fragment of the APP gene 5′-UTR inserted immediately in front of the CAT gene start codon. Briefly, the 3-kb *Sma*I fragment was cloned into the unique *Stu*I site of the pSV2 CAT expression vector to generate pSV2(APP1)CAT. DNA from pSV2(APP1)CAT was then truncated of coding sequences by *Nru*I and *Hin*dIII double digestion and ligation after dephosphorylation. The resulting construct encoded a CAT gene transcribed from the early T-antigen promoter with 90 nt (*Sma*I-*Nru*I APP 5′-UTR fragment) inserted into the 5′-UTR of the CAT reporter gene at a unique *Stu*I site.

The luciferase expression construct designated as pGAL encodes the complete 146-nucleotide 5′-UTR of the APP gene inserted as a PCR-generated DNA cassette in between the *Hin*dIII and *Nco*I sites in front of the luciferase gene in the pGL-3 vector (Promega, Madison, WI). Transfectants of pGAL transcribe a hybrid luciferase reporter that encodes the IL-1 responsive 90-nucleotide element described previously (9) and additional upstream 55 nucleotides immediately downstream from the 5′-cap site of APP mRNA.

The complete 1.2-kb APP 3′-UTR was cloned into a convenient *Xba*I site immediately downstream of the luciferase gene in the pGAL construct to generate pGALA. Hybrid APP-luciferase mRNAs expressed from pGALA transfectants transcribe the 146-nt APP 5′-UTR sequence element inserted upstream of the reporter gene start codon but also transcribes an additional 1.2 kb of APP 3′-UTR sequence downstream from the luciferase stop codon (11). Therefore the hybrid APP-luciferase mRNA expressed in pGALA transfectants exhibits the natural arrangement of APP gene 5′- and 3′-untranslated regions to provide an authentic representation of the non-coding regions of the precursor transcript.

The dicistronic construct, pJR-1, was prepared from the pIRES2 vector backbone (Clontech), which contained an internal ribosome entry site element (IRES) followed by enhanced green fluorescent protein gene. A PCR-generated DNA cassette encoding 146 bp of APP 5′-UTR was first cloned into the multiple cloning site of pIRES2 between unique *Xho*I/*Eco*RI sites. The downstream *Eco*RI/*Bam*HI sites were then used to ligate in the luciferase reporter gene (Luc; Promega, Madison, WI) or the RFP reporter gene (dsREDN-1; Clontech).

For RNA gel shift studies the pBS(APP) construct used for REMSA studies was prepared by inserting the 3-kb fragment of APP into the co-blunt-ended *Hin*cII site in pBS(sk+) vector (Stratagene) (see Fig. 6). Sense APP 5′-UTR cRNAs were transcribed using T3 polymerase with linearized *Nru*I-digested pBS(APP) as template. For experimental controls, T7 polymerase transcribed antisense transcripts from *Spe*I-digested pBSAPP template. A labeled 28-nt sense H-ferritin IRE transcript was transcribed from the pTHfer construct, which was a generous gift of Dr. Kuhn (Epingles, Switzerland) (32).

Transfections

Neuroblastoma cells (SY5Y) were transfected with 10 μg of DNA from the pGL-3, pGAL, and pGALA constructs and were co-transfected with 5 μg of DNA from a construct that expresses green fluorescent protein (GFP). Luciferase and GFP reporter genes were expressed from an SV40 promoter. Transfections were performed in the presence of LipofectAMINE-2000 according to the manufacturer's instructions (Invitrogen). Typically neuroblastoma cells were grown in flasks (100 mm^2) for each treatment. Each flask was transfected (12 h) and subsequently passaged equally into 96-well plates for exposure to chelators for 48 h (n = 5) for each treatment.

Desferrioxamine (50 mM stock in phosphate-buffered saline), clioquinol (50 mM stock in Me_2SO), and EDTA were each diluted 1/5000 to 1/50,000 into 2 ml of Dulbecco's modified Eagle's medium (without fetal calf serum) for 1 h at 37 °C to maximize solubility. Each individual concentration of chelators (100-μl volumes) was tested in triplicate or quadruplicate. After the treatment with each chelator for 36 h cell viability was established by a microscopic examination of each well. Cell viability was confirmed by relative expression of GFP in each 96-well by reading at 480/509-nm wavelength (GFP) using an automated Wallac 1420 multilabel counter. After obtaining a GFP readout the cells in each 96-well plate were lysed in 50 μl of reporter lysis buffer (Promega, Madison, WI) followed by luciferase assays using the Walac1420 counter.

Stable SH-SY5Y neuroblastoma transfectants were prepared using a construct, pJR-1, which transcribes a single dicistronic reporter mRNA. In this configuration, the RFP gene is under the translational control of APP 5′-UTR sequences (90-nt IL-1-responsive and baseline translational enhancer element) and a downstream GFP gene that is controlled translationally by an intergenic 5′-UTR IRES. Stably transfected neuroblastoma cells were exposed to increasing concentrations of desferrioxamine (1–100 μM) for 48 h, and RFP and GFP expression was then monitored by reading fluorescence as GFP = 480/509-nm and RFP = 558/583-nm wavelength. Intracellular iron chelation suppressed RFP gene expression in neuroblastoma cells. GFP served as an internal control to register the lack of responsiveness of the downstream IRES to increasing levels of iron chelation.

REMSA

In Vitro Transcription and Synthesis of RNA Probes of APP and H-ferritin 5′-Untranslated Regions—Ferritin IRE transcripts were prepared from a pBluescript construct, pTHfer (32), in which the human H-ferritin IRE region was encoded on the template DNA. The 56-base sense transcript encoding the canonical IRE (an experimental positive

control) was prepared with T7 RNA polymerase from *Bam*HI-digested pTHfer DNA. The pDAPP was used as template for the synthesis of APP transcripts encoding putative IRE-Type II sequences. Template DNA was digested with *Nru*I and transcribed with T3 to prepare [^{32}P]UTP-labeled sense APP transcripts containing 90 nt of APP 5′-UTR with an extra 25-nt pBS vector sequence at the 5′-end. *Spe*I-digested pBSAPP was used as a template for the preparation of antisense APP cRNAs for use as an experimental specificity control in REMSAs (see Fig. 8).

cRNAs encoding APP and H-ferritin 5′-UTR sequences were transcribed into labeled APP 5′-UTR transcripts (115 nt) (see Fig. 6*C*) and an H-ferritin IRE (pTFer) (32). DNA was transcribed in a 10-μl reaction volume with 1 unit of T7 or T3 RNA polymerase (Invitrogen) at 37 °C for 60 min in the presence of 100 μCi of [α-^{32}P]UTP (Amersham Biosciences), 2.5 mM each of rATP, rCTP, and rGTP (Amersham Biosciences), and 20 μM dithiothreitol. After preparation of labeled RNA probes the DNA template was digested with DNaseI prior to phenol extraction and ethanol precipitation. The labeled cRNA transcripts were size-separated by electrophoresis through 6% urea sequencing gels, and the full-length transcripts were eluted into 0.5 M ammonium acetate, 1 mM EDTA, 1 μM dithiothreitol, 10 μg tRNA, and 5 units of RNasin prior to phenol/chloroform extraction and by ethanol precipitation. Labeled RNA probes had a specific activity of 1–4 $\times$ 10^{10} cpm/μg RNA (30–50% incorporation), were resuspended in 80 μl of H_2O (treated with diethyl pyrocarbonate), and stored in aliquots at −80 °C.

For RNA electrophoretic mobility shift assays (REMSA), cytoplasmic extracts or recombinant IRP-1 were incubated with radiolabeled transcript (2–10 $\times$ 10^4 cpm, 2.5–10 pg) for 30 min at 22 °C in a reaction volume of 10 μl made up with cytoplasmic extraction buffer (33). In some reactions mouse polyclonal serum to IRP-1 or mouse pre-immune serum were included to generate supershifting complexes. Subsequently, RNase T1 (0–1 units) was added to the mixture for 10 min at 22 °C, followed by heparin (0–10 μg/μl) (Sigma) for 10 min at 22 °C. RNA loading dye (0.1 volume of 9% glycerol, 10 mg/ml bromphenol blue, and xylene cyanol; 5× TBE) was added to each sample. The RNA·protein complexes (RPC) were resolved at 4 °C for 15–20 min at 200 V in 0.5× TBE on a 1.5-mm 4–5% polyacrylamide mini-gel (Bio-Rad) (acrylamide:bisacrylamide ratio of 36:1 or 70:1) after pre-electrophoresis (200 V for 20 min; 0.5× TBE running buffer). After electrophoresis, gels were fixed in 10% isopropanol/7% acetic acid and vacuum-dried, and RNA-protein interactions were detected by use of a PhosphorImager (Molecular Dynamics, Sunnyvale, CA).

Competition between ferritin IRE and APP 5′-UTR transcripts were performed using 200-fold excess unlabeled transcript. In Fig. 8 the 115-nt ^{32}P-labeled APP 5′-UTR cRNA probe was transcribed from *Nru*I-digested pBSAPP DNA template (as above). We used a 200-fold excess of unlabeled cRNA probe and included tRNA to combat problems of input cRNA degradation. Competitor, at 200-fold excess, was used to test for specificity. Heparin and tRNA were included in reactions to ensure more specific detection of RNA-protein interactions.

RESULTS

Iron and the Control of APP Gene Expression at the Translational Level—Using neuroblastoma cells we performed Western blot analyses with an APP polyclonal antibody, C8 directed to the APP C terminus, to test whether cellular iron levels altered cellular APP protein levels and/or changed the amount of APP secreted into the conditioned medium of iron-treated cells. The APP antibody R1738 was used to detect secreted APP ectodomain. Fig. 1 (*Panel A*) shows a typical Western blot experiment where the C8 antibody detected the characteristic doublet of APP (molecular mass, 120–130 kDa) after fractionation by electrophoresis on a protein gel (12% SDS-PAGE gel). Intracellular APP levels were measured in experimentally treated triplicate flasks of SY5Y cells. The faster migrating band represents nascent APP, and the larger APP band is the glycosylated form of the precursor inside the cell (130 kDa) (34). Quantitation of the appropriate bands revealed that steady-state intracellular APP levels were decreased 2- to 3-fold by 50 and 250 μM desferrioxamine (Df). Exposure of SY5Y cells to 100 μM iron as FAC caused a 6-fold increase in the steady-state levels of cellular APP.

In *panel B*, Western blotting was used to detect the accumulated APP(s) levels secreted in the conditioned medium of neuroblastoma cells treated for 24 and 48 h with Df and iron (FAC) as described for *panel A*. The presence of 50 μM Df for 24 h reduced APP(s) levels to 50% of control whereas APP(s) levels were reduced a further 20% (<50% of control) after 48 h of exposure to the intracellular iron chelators (*Panel B*). Cell viability and growth were unchanged by these conditions.

The rate of APP protein synthesis was also markedly reduced under conditions of 24-h iron chelation of neuroblastoma cells (SY5Y cells) (*panel C*), in addition to altered steady-state levels of precursor. Three independent experiments showed that Df reduced [^{35}S]methionine incorporation into intracellular, immunoprecipitable APP (120 kDa). APP synthesis was reduced 4-fold after growth of cells for 24 h with desferrioxamine (*panel C* shows two of the separate experimental determinations). Our conditions for iron chelation with Df were sufficient to specifically suppress APP synthesis under conditions when cell viability was unchanged based on cell counts and a 3-(4,5-dimethylthiazol-2-yl)-2,5-diphenyltetrazolium bromide (MTT) assay (data not shown).

Steady-state levels of APP mRNA were unaffected by Df after 12 to 48 h of treatment of neuroblastoma cells, consistent with unchanged APP gene transcription (*panel C*). Using our conditions for Df administration to neuroblastoma cells, ferritin light and heavy subunit synthesis was selectively reduced whereas cell viability was unaffected. A similar pattern is observed in astrocytoma and hepatoma cells where interleukin-1 and iron stimulated both APP synthesis and ferritin synthesis (15, 36) without changing their mRNA levels. The discordance between APP mRNA and APP protein levels and the use of metabolic labeling to directly measure APP synthesis rates suggested that iron regulates APP gene expression at the level of message translation.

Panel D shows a typical transfection-based assay to test for the presence of iron-responsive activity in the APP 5′-UTR. Using the pSV2(APP)CAT construct, transfected neuroblastoma cells transcribed a chimeric APP/CAT mRNA with sequences from positions +54 to +145 from the 5′-cap site of the 146-nt 5′-UTR, including the stem loop. After pSV2(APP)CAT had been transfected into neuroblastoma cells, IL-1 elevated CAT gene expression by 3-fold, as reported previously (9). Iron (as 10 μM Fe_2Tf) also conferred a significant increase of APP CAT expression (pSV2CAT was shown previously to be unresponsive to both iron and IL-1 and iron (9). Iron induction was fully reversible by the co-treatment with Df (*panel D*). We concluded that 5′-UTR sequences in APP mRNA encoded a new iron-dependent translational regulatory element in addition to the IL-1-responsive acute box element.

A Putative IRE-Type II in the APP mRNA 5′-Untranslated Region—The iron and IL-1-dependent regulatory pattern for APP holoprotein expression shown in Fig. 1 had features in common with the translation of the L- and H-subunits of the iron storage protein, ferritin (9, 36). We computer-aligned APP 5′-UTR sequences with the known iron-responsive element in the 5′-UTR of the H-ferritin mRNA (Fig. 2) (Gap alignment program from the Genetics software packages (GCGdefs) compiled at the University of Wisconsin). Fig. 2*B* shows that an overall 67% identity was detected between APP 5′-UTR sequences (+51 to +94) and the 44-nt IRE in H-ferritin mRNA (+12 to +59) (*red lettering* in Fig. 7). Two clusters within the APP 5′-UTR (IRE-Type II subdomains) showed >70% identity with the ferritin IRE sequences. First a 16-base sequence in APP mRNA (+51 to +66) was found to be 72% similar to 5′-half of the H-mRNA IRE (+12 to +27). Second APP sequences (+82 to +94) (a 13-base cluster) were found to be 76% identical to the loop domain of ferritin IRE (+43 to +55). These IRE-Type II sequences in the APP 5′-UTR (+51 to +94) are sited immedi-

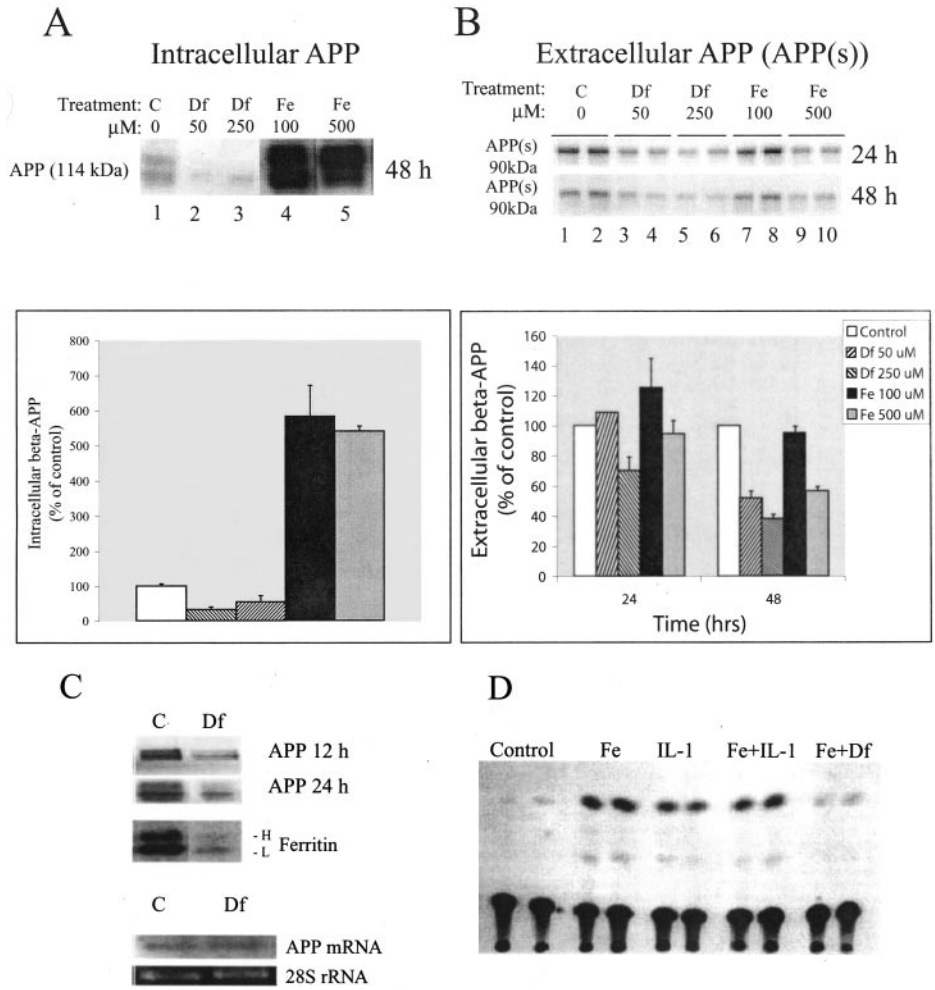

FIG. 1. **Iron regulates intracellular APP levels and the rate of APP translation.** *Panel A*, intracellular APP regulation in response to iron and desferrioxamine treatment of neuroblastoma cells (SH-SY5Y). Cells were treated for 48 h with Df and FAC. Cells were lysed and determined for protein content, after which 20 μg of cell extract was loaded on each *lane*. Proteins were fractionated by SDS-PAGE. Standardized Western blots were used to quantitate the steady-state levels of APP. The histogram graphically depicts the quantitation (n = 3) of the scans of the autoradiograms shown above. *Panel B*, extracellular APP (APP(s) levels in response to changed iron levels). Neuroblastoma cells were treated with FAC and Df for the indicated times. Cell medium was collected, medium was concentrated, and Western blots (R1753 antibody) were used to determine levels of APP(s) in the medium at 24 and 48 h post-induction. The histogram graphically depicts the quantitation (n = 3/expt, 3 expts) of the scans of the autoradiograms using densitometry by NIH Image software. *Panel C*, rate of APP protein synthesis relative to APP mRNA levels in neuroblastoma cells. Cells were exposed to Df (50 μM) for 12 and 24 h. After [^{35}S]methionine labeling for 30 min, cells were harvested and lysed, and the amount of intracellular APP synthesis was measured by autoradiography of SDS-PAGE fractionated proteins (as in *panels A* and *B*). APP mRNA levels were assessed by Northern blotting of parallel Df-stimulated cells. *Panel D*, the 90-bp *Sma*I-*Nru*I APP 5′-UTR fragment, including the IRE homology domains, confers increased translation to a CAT reporter by IL-1 and iron. Neuroblastoma cells were transfected with pSV2(APP)CAT construct. After equal passage, cells were exposed for 24 h to (i) iron (as 10 μM $Fe_2$2Tf), (ii) IL-1β, (iii) IL-1β and Fe_2Tf (10 μM), and (iv) Fe_2Tf (10 μM) and Df (25 μM), and CAT assays were performed as indicated under "Experimental Procedures."

ately upstream of the IL-1 acute box domain in the APP 5′-UTR (+101 to −146) (9).

The fold program of Zuker (37) (bioinfo.rpi.edu) was used to predict the best thermodynamic folding structure for the 146-nt APP 5′-UTR sequence element. This predicted APP RNA stem loop is shown in *panel A* with a Gibbs free energy value of −54.6 kcal/mol. The 11-nucleotide loop region was found to align with 75% sequence identity with the ferritin IRE stem loop (*bold lettering* represents nucleotides +83 to +93 in the loop region of APP mRNA, corresponding to the second boxed homology domain (*panel B*).

In *panel D* a set of separate pSV2(APP)CAT-based transfections showed that IL-1 and Fe_2Tf (10 μM) treatment (12 h) induced CAT reporter gene expression by >3-fold. In this experiment transfected CAT expression was assayed using a liquid scintillation CAT diffusion assay as we described previously (36). The transcription rates of the CAT gene in pSV2(APP)CAT transfectants was unaltered in response to IL-1 and iron in neuroblastoma cells, because RNase protection analysis showed that APP CAT mRNA levels were not altered by IL-1 or iron treatment (*panel C*).

The APP 5′-UTR Encodes a Functional Iron-responsive Element—Because APP 5′-UTR sequences are homologous to the ferritin IREs, and because APP is regulated by iron and binds to both iron and copper (3), we tested the relative capacity of the iron chelator, desferrioxamine, to suppress APP 5′-UTR-driven translation of a second reporter gene. For the purpose of maximizing specificity a construct was designed to express two reporter genes transcribed in a single dicistronic mRNA from one cytomegalovirus promoter. The upstream RFP gene was expressed under the control of APP 5′-UTR sequences, encoding the 90-nt APP 5′-UTR translation enhancer element, with an IRE. On the same dicistronic transcript the downstream GFP was translated under the control of a viral IRES (38). In

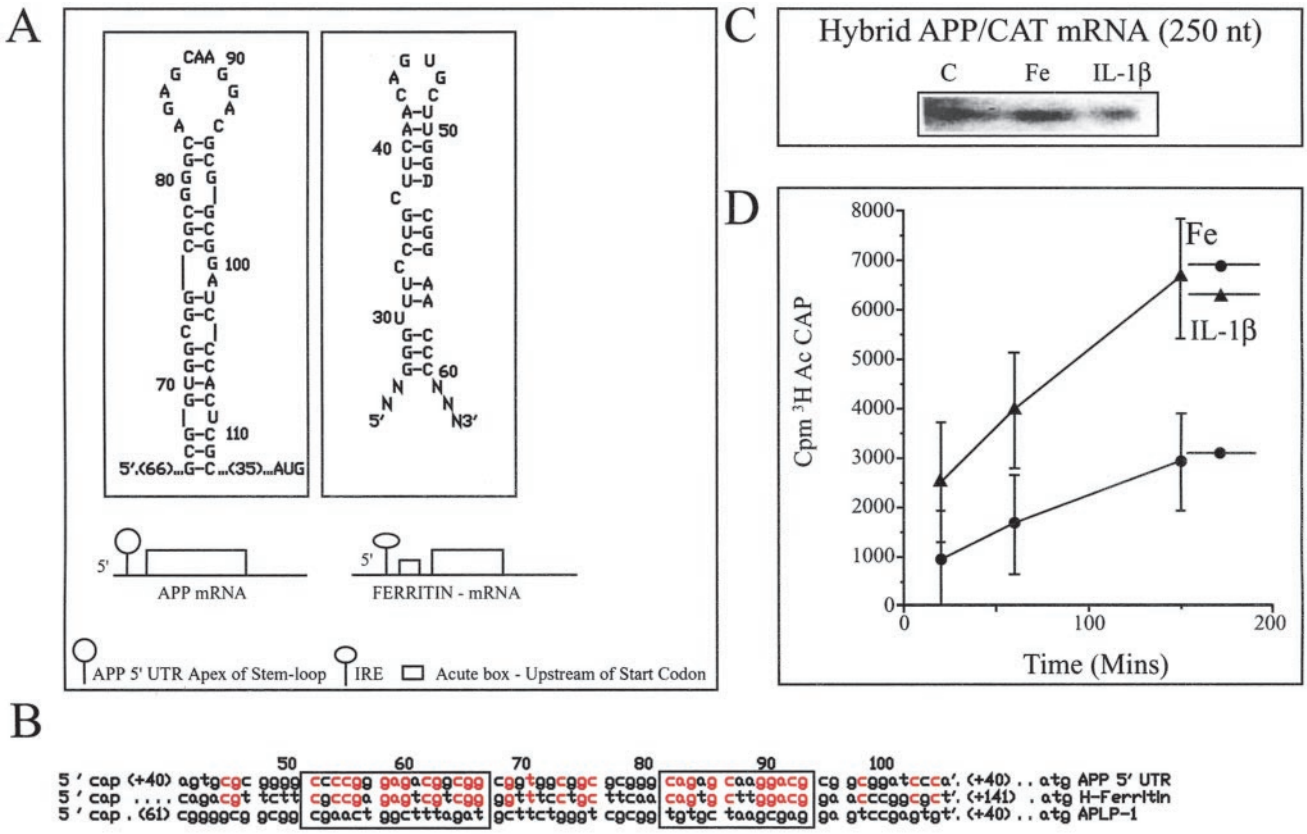

FIG. 2. **Evidence for an iron-responsive element in the 5′-UTR of APP mRNA.** *Panel A*, APP 5′-UTR sequences were computer-folded to generate the predicted RNA stem loop shown (*left* RNA secondary structure, Gibbs free energy = 55 kcal/mol) (Zuker *et al.* (37), Rogers *et al.* (9)). *Bold lettering* shows the homology with the H-ferritin IRE (*right* RNA secondary structure) (Thomson *et al.* (20)). *Panel B*, homology exhibited between the H-ferritin mRNA IRE and APP 5′-UTR sequences. Computer-based alignments (Gap, GCGDefs; University of Wisconsin) revealed an overall 66% similarity exists between APP 5′-UTR sequences (+51 to +94) and the 44-nt IRE in H-ferritin mRNA (+12 to +59) (shown in *red lettering*). Two homology clusters exist (*boxed regions*) in this APP IRE-Type II, which are shown to display >70% homology with ferritin IRE sequences as follows: (i) a 16-base sequence in APP mRNA (+51 to +66) is 72% similar to 5′-half of the H-mRNA IRE (+12 to +27); (ii) APP sequences (+82 to +94) constitute a 13-base cluster that is 76% homologous with the loop domain of the Ferritin IRE (+43 to +55). IRE-Type II sequences in the APP 5′-UTR (+51 to +94) are sited immediately upstream of the IL-1 acute box domain in the APP 5′-UTR (+101 to −146) (Rogers *et al.* (9)). As a specificity standard, APLP-1 5′-UTR sequences exhibit 25% similarity to APP (shown) and APLP2 (not shown) as predicted from the alignment of related genes (5′-UTR sequences diverge more rapidly than coding sequences). APLP-1 5′-UTR sequences exhibited no homology with the H-ferritin IRE (APLP-1 is not regulated by intracellular iron chelation). *Panel C*, neuroblastoma cells were transfected with DNA from the pSV2(APP)CAT construct. After equal passage cells were exposed for 24 h to iron (as 10 μM Fe_2Tf) or IL-1β or left untreated. Cells were assayed for CAT activity (0.2 vol) (*panel D*), or RNase Protection analysis was performed using a pBSCAT-generated cRNA probe as described previously (*panel C*) (21).

this configuration, both the RFP and GFP genes could be expressed at stoichiometrically equivalent levels on the same plasmid from the same cytomegalovirus promoter.

Fig. 3 shows a representative transfection-based experiment (n = 3) wherein iron chelation with Df specifically targeted the 90-nucleotide *Sma*I-*Nco*I element in the APP 5′-UTR to cause suppression of the downstream RFP reporter translation. A critical finding was that Df did not suppress downstream GFP expression. GFP was translated from the same dicistronic transcript as RFP but was synthesized under the control of an IRES. GFP expression was unchanged over the 1–100 μM dose range of Df. Intracellular iron chelation by Df suppressed APP 5′-UTR-driven translational control of the RFP by 20% after a 48-h treatment of stable transfectants with 1 μM DFO. Over increasing doses of Df, the percent reduction in RFP expression diminished by 40% (60% of control values using 80–100 μM desferrioxamine). The lack of inhibition of GFP expression, driven by an IRES on the same transfected transcript, provided us with clear evidence that the APP 5′-UTR is an IRE-Type-II-responsive element that mediated the action of Df to limit downstream translation. Maintenance of control levels of GFP demonstrated that Df does not cause cytotoxicy in neuroblastoma cells. These stably transfected cells were "growth-positive" under all levels of iron chelation used. In sum, iron chelation with Df selectively and dose-dependently (1–100 μM) suppressed APP 5′-UTR-specific translational expression of RFP.

Desferrioxamine Specifically Suppresses APP 5′-UTR-directed Translation of Luciferase Reporter mRNAs—In Fig. 4 only constructs expressing APP 5′-UTR (+146 nt) exhibited a reduction of downstream APP-luciferase reporter mRNA translation in response to intracellular iron chelation. Df (10–30 μM) selectively inhibited luciferase expression only in pGAL transfectants (+146 nt of APP 5′-UTR) whereas the same concentrations of chelator (30 μM Df) left luciferase mRNA translation unchanged in pGL-3 transfectants that lack the 146-nt APP 5′-UTR cassette. These transfection-based studies confirmed that the APP 5′-UTR is a baseline translational enhancer (3-fold higher luciferase expression relative to pGL-3) that is dose-responsive to the intracellular iron chelation (10−30 μM doses; n = 5).

The transfection assay shown in *panel B* confirmed that desferrioxamine also selectively inhibited by 3-fold chimeric APP luciferase mRNA translation through APP 5′-UTR sequences (pGAL construct) and in the additional presence of the downstream APP 3′-UTR (1.2 kb) element (pGALA construct). In all the transient transfections with the pGL-3, pGAL, and

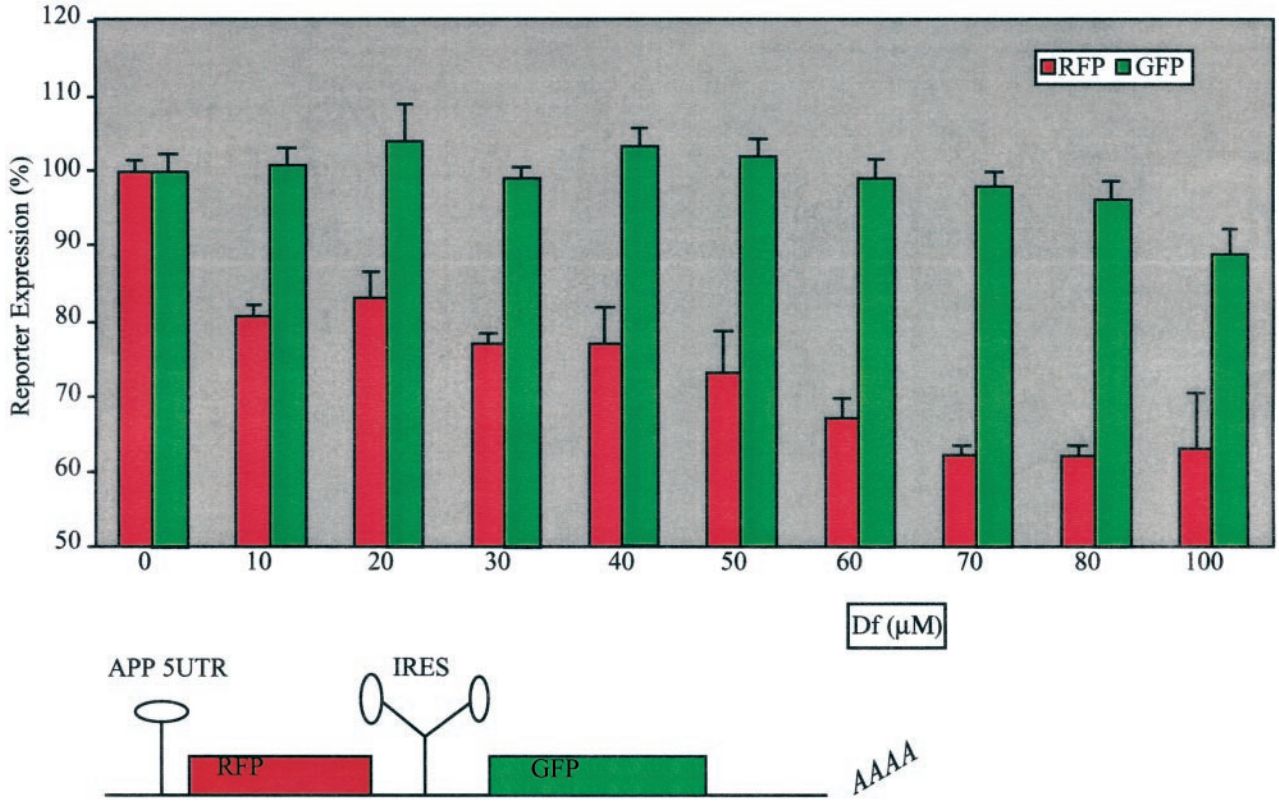

FIG. 3. **Desferrioxamine selectively inhibits APP 5′-UTR-driven translation of an RFP reporter downstream but exerts no effect on translation of a dicistronic GFP reporter gene controlled by a viral internal ribosome entry site.** Neuroblastoma cells, stably transfected with pJR-1, were exposed to increasing concentrations of desferrioxamine for 48 h. Both RFP and GFP expression was then monitored by reading fluorescence at 400 nM wavelength (RFP) and 500 nM wavelength (GFP). GFP served as an internal control to register the lack of responsiveness of the downstream IRES to increasing levels of iron chelation. Maintenance of control levels of GFP expression demonstrated that desferrioxamine does not cause neurotoxicity. Experimentally the SY5Y neuroblastoma cells were transfected with 10 μg of plasmid and selected for neomycin resistance to establish stable lines. After passage Df concentrations were added to 96 wells (n = 8 wells for each concentration) over incrementally increased concentrations of iron chelator (1–100 μM) for 48 h. The stably transfected cell line was growth-positive under all levels of iron chelation used.

pGALA plasmids the luciferase gene was transcribed from the common SV-40 early T-antigen promoter, which is not iron-responsive (36). Because these transfection data are standardized with co-transfected GFP expression plasmid, the observed differences in baseline luciferase expression can only be accounted for by the capacity of the chelators to suppress enhanced baseline reporter mRNA translation conferred by UTR sequences (pGALA > pGAL > pGL-3).

APP 5′-UTR-directed Translation Is Specifically Inhibited by Intracellular Metal Ion Chelation But Not in Response To the Extracellular Cation Chelator, EDTA—Fig. 5 shows similar transient transfection-based assays where we measured the specificity and degree to which (i) Df (high affinity iron chelator), (ii) clioquinol (low-affinity copper-zinc-iron) chelator, and (iii) EDTA (extracellular Ca^{2+} and Mg^{2+} chelator) suppressed APP 5′-UTR directed translation of a luciferase reporter mRNA (using pGAL, pGALA, and pGL-3). Operationally the transiently transfected cells were passaged into four duplicated rows of a 96-well plate and then exposed to (i) Df (1 to 100 μM), (ii) matching concentrations the divalent copper-zinc chelator, clioquinol (1 to 100 μM in the adjacent three rows), and (iii) the non-metal-specific divalent cation chelator, EDTA (1 to 100 μM in the adjacent three rows). To ensure equal experimental transfection efficiency in all experiments luciferase activity was standardized by assessing the levels of co-transfected GFP activity. A dose-response chelator-inhibition curve was set up using the average luciferase activity measured in four separate wells per drug dose. Each point is the average of four separate wells for generating the dose-response curves in Fig. 5.

Extrapolation from the dose-response curve in Fig. 5*A* showed that 10 μM Df chelated sufficient intracellular iron to selectively inhibit half of APP 5′-UTR-driven expression of luciferase mRNA translation (IC_{50} = 10 μM in pGAL transfectants). To control for specificity the extracellular divalent Mg^{2+} and Ca^{2+} chelator EDTA exerted no suppression of translation through APP 5′-UTR sequences. The lack of EDTA effect provides an additional specificity control for our conclusion that only the intracellular metal chelators, Df and clioquinol, suppress APP 5′-UTR-dependent translation. The copper-zinc-iron chelator, clioquinol, inhibited APP 5′-UTR-conferred translation of the downstream luciferase reporter in transient pGAL transfectants with an IC_{50} of 21 μM. The dose-response experiments shown in Fig. 5 are representative of multiple independent determinations (n = 4). The IC_{50} values for each chelator to inhibit transfected APP/luciferase gene expression was calculated from the inhibition curves and is shown in Table I (n = 4). Table I summarizes the IC_{50} values for the desferrioxamine and clioquinol to specifically suppress translation conferred by the 146-nt APP 5′-UTR element (pGAL) (IC_{50} = 10 μM for desferrioxamine, IC_{50} = >21 μM for clioquinol).

Labeled APP 5′-UTR Transcripts Selectively Interact with Iron-regulatory Proteins—We used a standard REMSA to test for a possible interaction between labeled cRNAs encoding 5′-UTR sequences in the APP mRNA and recombinant IRP-1. The pBS(APP) construct used to generate labeled cRNAs is shown in *panel A* (Fig. 6). In the REMSA shown in *panel B*, inclusion of a mouse antibody to rIRP-1 generated a supershift of the RNA·protein complex (RPC) and a reduction in the

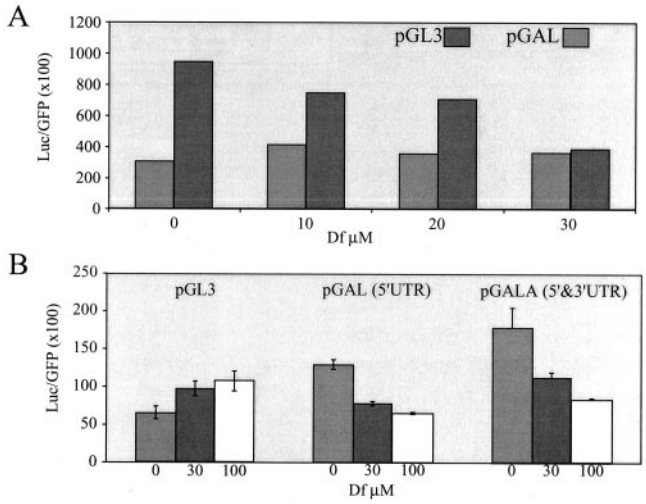

FIG. 4. **Desferrioxamine selectively inhibits the capacity of the APP 5′-UTR to confer baseline translation to a luciferase reporter mRNA.** *Panel A*, the pGAL construct expresses APP 5′-UTR sequences inserted in front of the luciferase gene start codon within the unique 5′-UTR *Hin*dIII/*Nco*I sites of the luciferase gene in the parental pGL-3 vector (Promega, Madison, WI). DNA from pGAL and pGL-3 (10 μg) was transiently transfected into SY5Y neuroblastoma cells in the presence of standardizing GFP plasmid (5 μg). Transfected cells were split equally into four flasks and grown in duplicate for 36 h as follows: (i) untreated, (ii) 10 μM Df (DFO), (iii) 20 μM Df (DFO), and (iv) 30 μM Df (DFO). To standardize for transfection efficiency cells were washed in phosphate-buffered saline and quantitated for GFP activity. Cells were then lysed (1× reporter gene lysis buffer; Roche Molecular Biochemicals), and the lysates were monitored for luciferase activity. The *graphs* show the effect of iron chelation with Df (DFO) to suppress luciferase gene expression in pGAL transfectants (+APP 5′-UTR). Transfectants of pGL-3 (−APP 5′-UTR) were unresponsive to iron chelation with desferrioxamine. Values on the *y* axis were standardized to account for minor differences in the transfection efficiencies between pGAL and pGL-3 plasmids (n = 6). *Panel B*, transfection assays were performed as described in *panel A*, but the effect of Df on luciferase expression in pGALA transfectants (APP 5′-UTR + APP 3′-UTR sequences) was also monitored.

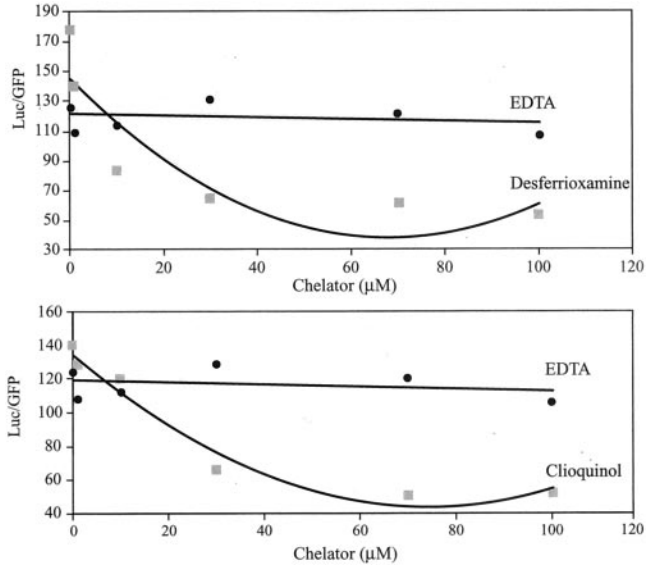

FIG. 5. **Translation by the APP 5′-UTR enhancer is responsive to intracellular iron and copper chelation but not Ca^{2+} and Mg^{2+} chelation.** *Panel A*, dose-responsive iron chelation with desferrioxamine suppressed APP 5′-UTR conferred translation of a downstream luciferase reporter mRNA (pGAL) whereas the same concentrations of EDTA did not reduce luciferase expression. pGAL-transfected SY5Y cells were split equally into a 96-well format (n = 4), and cells were grown in the presence of increasing concentrations of desferrioxamine (1–100 μM) for 48 h. After harvesting lysates, differences in transfection efficiency were standardized by expression of a co-transfected GFP gene (5 μg of co-transfected GFP plasmid with 10 μg of pGAL plasmid). The potent inhibitory action of desferrioxamine on chimeric APP/luciferase reporter expression was evaluated statistically by linear regression (best fit curves shown in the *graphs*). The IC_{50} (half-inhibitory concentration) of desferrioxamine required to reduce maximal APP 5′-UTR-driven translation was presented in Table I. EDTA (n = 3) did not inhibit the translation of luciferase reporter mRNA driven by APP 5′-UTR sequences. *Panel B*, dose-responsive metal chelation with clioquinol suppressed APP 5′-UTR conferred translation of a downstream luciferase reporter mRNA (pGAL). As shown in *panel A* the same concentrations of EDTA did not reduce luciferase expression. pGAL-transfected SY5Y cells were split equally into a 96-well format (n = 4), and cells were grown in the presence of increasing concentrations of clioquinol (1–100 μM) for 48 h. After harvesting lysates, differences in transfection efficiency were standardized by expression of co-transfected GFP (5 μg of co-transfected GFP plasmid with 10 μg of pGAL plasmid). The potent inhibitory action of clioquinol on chimeric APP/luciferase reporter expression was statistically evaluated by linear regression (bestfit curves shown in the *graphs*). The IC_{50} (half-inhibitory concentration) of clioquinol required to reduce maximal APP 5′-UTR-driven translation is presented in Table I. As shown in *panel A*, EDTA (n = 3) did not suppress APP 5′-UTR-driven translation of a downstream chimeric APP/luciferase reporter mRNA in these transfection-based assays.

TABLE I

Half-inhibitory concentrations (IC_{50}) of chelators to reduce APP 5′-UTR-driven translation (n = 5/assay) (four separate transfections)

Construct/chelator	pGAL (5′-UTR)
	μM
Desferrioxamine (iron chelator)	10
Clioquinol (copper chelator)	21
EDTA (Ca^{2+} and Mg^{2+} chelator)	>>>30

amount of APP/IRP formed (compare *lanes 2* and *3*). Inclusion of anti-IRP-1 antibody also generated a supershift of the RPC formed between APP 5′-UTR and a neuroblastoma lysate protein (compare *lanes 4* and *5* and *lanes 6* and *7*). Because anti-IRP-1 antibody generated a specific supershifted complex, these data demonstrated that the APP 5′-UTR interacted with both recombinant IRP-1 and an RNA-binding protein related to IRP in neuroblastoma lysates. The supershifted band for recombinant IRP-1 reproducibly migrated slightly in advance of the supershifted complex formed when using lysate proteins. This effect is reproducible and may be the result of the involvement of other APP 5′-UTR RNA-binding proteins.

The REMSA in Fig. 6*D* shows that antiserum raised against rIRP-1 from a second mouse generated the same specific RNA·protein complex (compare *lanes 1* and *3* with *lanes 2* and *4*). Pre-immune serum from matching mice did not supershift the RPC formed between APP 5′-UTR and neuroblastoma IRP (compare *lanes 3* and *4*). In other RNA gel shifts (n = 6) the APP 5′-UTR probe did not bind to antibody alone (not shown).

In Fig. 6*C* labeled 90-nt cRNA for APP 5′-UTR (*Sma*I-*Nru*I) formed an RPC with recombinant IRP-1 and lysate IRP (*lanes 2* and *3*) (*bottom panel*) that co-migrated with the RPC formed between the ferritin IRE and rIRP-1 (*top panel*). *Lane 1* of both panels represents no protein; *lanes 2* and *3* include rIRP-1 (10 ng) in the reactions (33). On the same 4% acrylamide gel, labeled cRNAs encoding both the ferritin IRE and APP 5′-UTR sequences also formed a specific RPC with neuroblastoma IRP-1/2 (*lanes 4* and *5*, both *panels*). The RPCs formed between cRNA probes and recombinant IRP-1 migrated more slowly than lysate IRP complexes, because the recombinant His-tagged IRP-1 truncated 30 amino acids at the amino terminus (40).[2]

Lysates derived from IL-1-stimulated cells showed more complex formation (*lanes 6* and *7*) relative to control cells (*lanes 4* and *5*) (n = 3). Lysates from Df-treated cells showed reduced complex formation (compare *lanes 4* and *8*) (n = 3). The ferritin

[2] A. Koeppen, personal communications.

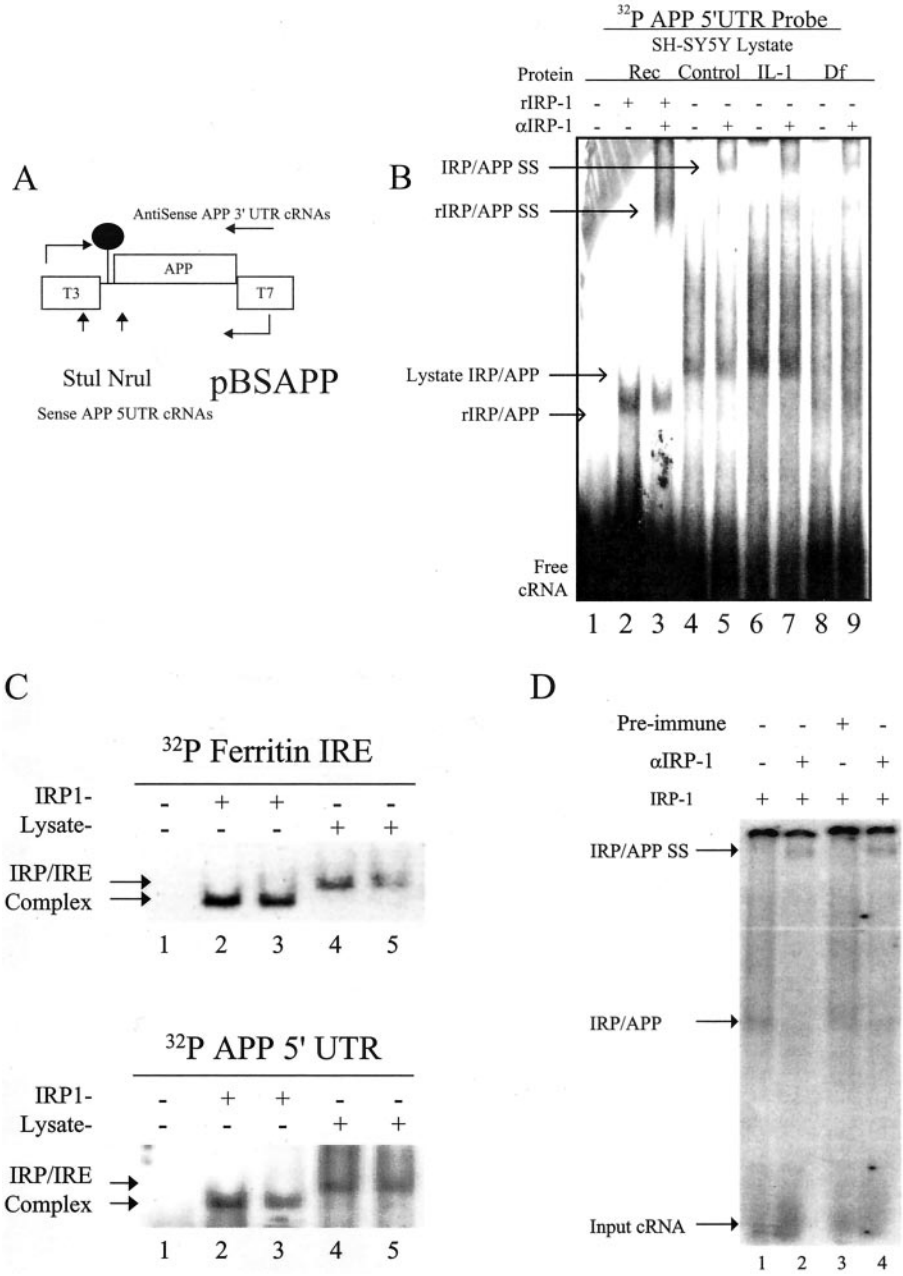

FIG. 6. **Specific interaction between APP 5′-UTR (IRE-Type II) and iron-regulatory proteins.** *Panel A*, constructs used to generate labeled APP and ferritin 5′-UTR probes. Transcripts for the APP 5′-UTR were synthesized using T3 polymerase and an *Nru*I-digested pBSAPP DNA template. Ferritin cRNAs were made from a pTHfer template (39). *Panel B*, labeled APP 5′-UTR cRNAs bind to rIRP-1 and neuroblastoma IRPs to form an RNA·protein complex that can be supershifted with IRP-1 antibody. Lysates prepared from desferrioxamine- and IL-1-treated cells exhibited modulated binding of the APP 5′-UTR probe to lysate IRP. *Lane 1*, APP 5′-UTR cRNA probe; *lane 2*, IRP-1 and APP 5′-UTR cRNA probe; *lane 3*, supershifted version of *lane 2* with anti-IRP-1 antibody; *lane 4*, untreated SY5Y lysate; *lane 5*, supershifted version of *lane 4* with anti-IRP-1 antibody; *lane 6*, IL-1-stimulated SY5Y lysate; *lane 7*, supershifted version of *lane 6* with anti-IRP-1 antibody; *lane 8*, lysate from Df-treated cells; *lane 9*, supershifted version of *lane 8* with anti-IRP-1 antibody. *Panel C*, ^{32}P-labeled cRNAs encoding APP 5′-UTR sequences (APP-cRNA) specifically interact with recombinant IRP-1 and lysate IRP to form an RNA-binding complex (RPC) that co-migrates with the RPCs formed between the ^{32}P-labeled ferritin-IRE and IRP-1 (representative of eight separate assays). *Panel D*, ^{32}P-labeled cRNAs encoding APP 5′-UTR sequences (APP-cRNA) specifically interact with lysate IRP to form an RNA-binding complex (RPC) that is supershifted by mouse antiserum raised against rIRP-1 (*lanes 2* and *4*) but not by pre-immune serum (*lane 3*) and in reactions with no antibody (*lane 1*).

IRE is known to interact more strongly with IRP-1 and/or IRP-2 after desferrioxamine exposure to cells (39). For APP mRNA iron chelation with desferrioxamine reduced the interaction between IRP-1 and APP 5′-UTR probe (Fig. 6*B*). IL-1 increased the interaction (Fig. 6*B*).

The RNA gel-shift experiments shown in Fig. 7 demonstrate that a deletion of the second IRE homology domain in APP 5′-UTR significantly reduced the interaction between rIRP-1 and the APP 5′-UTR. These findings supported our model that the APP 5′-UTR encodes an active iron-responsive element (IRE-Type II). Mutant APP 5′-UTR transcripts were generated with a deletion of the region of the APP 5′-UTR predicted to be homologous to the core CAGUGN loop region of the H-ferritin iron-responsive element (nucleotides +83 to +86 were deleted as shown in Fig. 7). In *lanes 1* and *2* ferritin IREs bound rIRP-1 and lysate IRP to form a specific RPC (*lanes 1* and *2*). Labeled transcripts encoding the APP 5′-UTR also showed specific binding to rIRP-1 (*lane 6*) and binding to an IRP in SY5Y lysate (*Lane 5*) although at reduced levels compared with the known high affinity with which the ferritin IRE interacts with IRP-1. RNA gel shifts using APP cRNA bearing the Δ4 mutation (Δ4 cRNAs) only bound weakly to form a specific RPC with recombinant IRP-1 (*lane 4*). There was no detectable binding between the Δ4 cRNAs and lysate IRPs (*lane 3*).

Densitometry showed that interaction between IRP-1 and Δ4 mutant cRNAs was reduced 10-fold compared with the binding of the wild-type APP 5′-UTR probe and rIRP-1 (compare *lanes 4* and *6*). When using recombinant IRP-1 the Δ83–86 mutant APP 5′-UTR reproducibly exhibited residual binding (*lane 4*) but displayed no binding to lysate IRP (*lane 3*). This observation probably resulted from IRP-1 binding to sequences in the upstream homology domain (see "Discussion"). The differential mobility between the ferritin IRE·IRP complex and APP 5′-UTR·IRP complex evident in Fig. 6 is not shown in Fig. 7. The regions of significant homology between the APP 5′-UTR are presented in *red lettering* (Fig. 7, *lower panel*), the two APP 5′-UTR IRE domains are *boxed*, and the deleted nucleotides are shown relative to the second IRE domain.

In Fig. 8 our results showed that the ferritin IRE transcripts cross-competed with labeled APP 5′-UTR probe for binding to

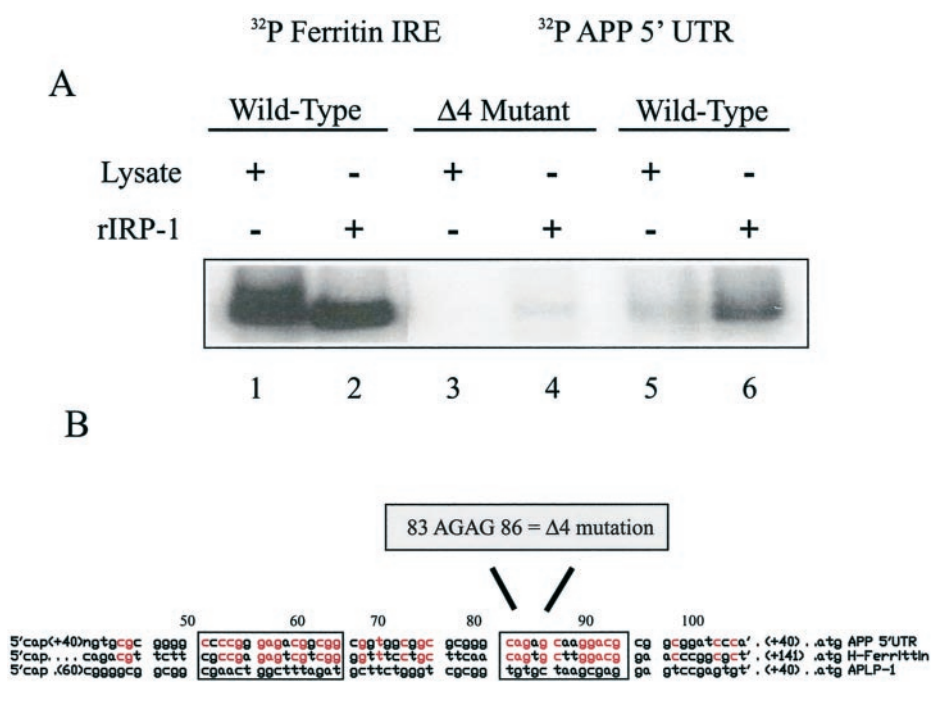

FIG. 7. **Deletion mutation of the second IRE homology domain reduces the interaction between iron-regulatory proteins and the APP 5′-untranslated region *in vitro*.** A labeled transcript encoding a 4-base deleted mutant version of the APP 5′-UTR no longer binds to lysate IRP and exhibited reduced specific binding to recombinant IRP-1. *Lane 1*, ^{32}P-labeled ferritin IRE cRNA probe with IRP in human neuroblastoma lysate (SY5Y·5 μg); *lane 2*, ^{32}P-labeled ferritin IRE with rIRP-1 (10 ng); *lane 3*, ^{32}P-labeled Δ4 mutant APP 5′-UTR cRNA probe with human neuroblastoma lysate (SY5Y; 5 μg); *lane 4*, ^{32}P-labeled Δ4 mutant APP 5′-UTR probe with rIRP-1 (10 ng); *lane 5*, ^{32}P-labeled APP 5′-UTR cRNA probe with human neuroblastoma lysate (SY5Y; 5 μg); *lane 6*, [^{32}P]-labeled APP 5′-UTR cRNA probe with rIRP-1 (10 ng). *Panel B*, the APP IRE (Type II) homology domains are depicted in *red lettering* and are *boxed*. APP sequences were mutated between nucleotides from +83 (AGAG) to +86 (Δ4 mutant) so that deleted APP 5′-UTR transcripts could be transcribed. The deletion corresponded to the first four bases of the loop region of the predicted APP 5′-UTR RNA stem loop structure shown in Fig. 2.

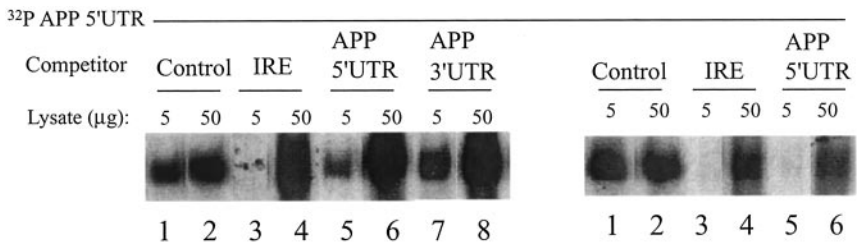

FIG. 8. **Transcripts encoding the H-ferritin IRE cross-competed with ^{32}P-labeled APP 5′-UTR cRNA probes for binding with neuroblastoma and hepatoma lysate proteins.** *Panel A*, SH-SY5Y lysates. H-ferritin IRE (200× excess) prevented (100%) labeled APP cRNAs from binding to lysate IRP (compare *lanes 1* and *3*). A similar 200× excess of unlabeled APP cRNA 75% competed with labeled APP cRNA for formation of a specific RPC with SY5Y lysates (compare *lanes 1* and *5*). As a control for specificity APP 3′-UTR sequences (200× molar excess) did not compete with labeled APP 5′-UTRcRNA probe for formation of a specific RNA-binding complex (RPC) in SH-SY5Y lysates (compare *lanes 1* and *7*). *Lanes 2*, *4*, *6*, and *8*, the ^{32}P-labeled APP 5′-UTR probe was reacted with 50 μg of lysate (saturated binding observed, equivalent to input probe). *Panel B*, HepG2 lysates. H-ferritin IRE (200× excess) prevented 100% labeled APP cRNAs from binding to lysate IRP (compare *lanes 1* and *3*). A similar 200× excess of unlabeled APP cRNA 100% competed with labeled APP cRNA for formation of a specific RPC in SY5Y lysates (compare *lanes 1* and *5*).

IRP when using either neuroblastoma (SY5Y) or hepatoma (HepG2) cell lysates ($n = 8$; <5 μg of lysate). These data support the conclusion that APP 5′-UTR sequences interacted specifically with an iron-regulatory protein. A 200-fold excess of unlabeled APP 5′-UTR cRNA partially competed with labeled APP cRNA for formation of a specific RPC in neuroblastoma lysates (*panel A*, *lane 5*) but completely competed for binding in hepatoma lysates (*panel B*, *lane 5*). The H-ferritin IRE cross-competed with labeled APP 5′-UTR as effectively as the homologous APP 5′-UTR cRNA for preventing binding of the APP 5′-UTR probe to both neuroblastoma (*panel A*, *lane 3*), and hepatoma lysate factors (*panel B*, *lane 3*). To control for specificity of competition, antisense transcripts encoding APP 3′-UTR sequences did not compete with the labeled APP 5′-UTR probe to form a specific RPC (*panel A*, *lane 7*). These results suggest that the APP 5′-UTR binds to IRP-1 and/or IRP-2 *in vivo*, in addition to specifically interacting ($n = 9$) with recombinant IRP-1 *in vitro*.

DISCUSSION

This report shows the presence of a functional iron-regulatory element (IRE-Type II) in the 5′-UTR of the mRNA encoding the Alzheimer's APP. We showed previously that IL-1 stimulated 12-fold increase in the rate of astrocytic APP protein synthesis through APP 5′-UTR sequences (9). In that same report, iron levels were also shown to regulate APP mRNA translation in astrocytic cells (9), consistent with the current results in which intracellular iron levels significantly modulated APP synthesis in neuroblastoma cells (Fig. 1). APP(s) secretion reflected intracellular APP levels in response to desferrioxamine treatment (Fig. 1, *panels A* and *B*). However iron may decrease α-secretase cleavage rates, because 24- and 48-h stimulation with ferric ammonium citrate (500 μM) reduced APP(s) levels at the same time that intracellular APP levels were enhanced significantly.

Sequences within the APP 5′-UTR conferred iron-dependent regulation to three separate reporter genes (CAT, luciferase, and RFP reporters; see Figs. 2–5). RNA gel-shift data confirmed that APP 5′-UTR sequences bound specifically to recombinant IRP-1. The interaction between lysate IRP and APP 5′-UTR sequences was reproduced using neuroblastoma lysates such that a 200-fold excess presence of H-ferritin IRE cross-competed the interaction as effectively as unlabeled homologous APP 5′-UTR transcript. The interaction was also supershifted using anti-IRP-1 antiserum. The finding that pre-

immune serum no longer generated the supershifted complex (Fig. 6*D*) provide an important selectively control to validate the antibodies raised against rIRP-1.

We concluded that the RPC formed after the binding of IRP-1 to APP 5′-UTR sequences was highly specific, because the RPC was supershifted readily and cross-competed by unlabeled ferritin IRE sequences. Binding to recombinant IRP-1 and a lysate IRP was abrogated by the presence of a deletion mutation in the loop region homology domain-2. In Fig. 7 there remains residual binding between the mutant APP 5′-UTR cRNA and recombinant IRP-1 (10-fold less than wild-type). We suggest the maintenance of residual binding was probably the result of interaction between the upstream IRE homology domain in the 146-nt APP 5′-UTR (+51 to +66) and rIRP-1. When using neuroblastoma lysate, other RNA-binding protein interactions to the APP 5′-UTR override the capacity to observe residual binding as seen in *lane 3* of Fig. 7. These data lend further support to the model that APP 5′-UTR sequences interact specifically with an iron-regulatory protein in human neuroblastoma and hepatoma cells.

The active element was designated as an IRE-Type II, because labeled cRNAs encoding the APP 5′-UTR showed a different modulated binding to IRPs relative to labeled H-ferritin IRE transcripts (Fig. 6). Desferrioxamine decreased the specific interaction between APP 5′-UTR cRNA probes and neuroblastoma lysate IRP whereas the interaction between hepatic IRP-1 and IRP-2 and the ferritin IRE is known to be increased significantly in response to intracellular iron chelation (39). The RNA gel-shift data showed that the APP IRE-Type II exhibited modulated binding to IRP-1/IRP-2 similar to IRE-like sequences in the 5′-UTR of the mRNA encoding transferrin (Tf RNA) (41). However Tf mRNA 5′-UTR sequences were shown to bind at higher affinity to lysates derived from cells exposed to iron chelation with desferrioxamine (41).

The finding that 5′-UTR sequences in both APP and ferritin mRNAs are baseline translation enhancers (Fig. 4) differs from the mechanisms governing translation of most eukaryotic mRNAs. For example, the transcript for FMR protein (fragile X mental retardation protein) encodes 5′-UTR secondary structure that is sufficiently stable to suppress downstream FMR protein translation (42). APP 5′-UTR RNA sequences are predicted to fold into an RNA stem loop with a Gibbs free energy value ($\Delta G = -54.9$ kcal/mol (9)) that would also be expected to suppress translation of a downstream start codon. However the 146-nt APP 5′-UTR conferred increased baseline translation to reporter mRNAs in neuroblastoma and astrocytoma cells similar to ferritin L- and H-mRNAs in hepatoma cells (9, 36). The data in Fig. 4*A* show that pGAL transfectants exhibited >3-fold elevated luciferase expression compared with luciferase expression from pGL-3 transfectants (in pGAL the full-length 146-nt APP 5′-UTR was inserted immediately in front of the luciferase gene start codon from pGL-3).

IRE-dependent pathways govern the post-transcriptional expression of many proteins involved in iron metabolism, in addition to ferritin and the transferrin receptor. For example erythroid aminoluvenyl synthase mRNA encodes a 5′-UTR cap site-specific IRE and is translated more efficiently during iron influx into reticulocytes, leading to enhanced heme biosynthesis during red blood cell production (43). Also, the iron transporter gene encoding IREG1/ferriportin is crucial for the movement of iron from the gut into the blood and is known to encode functional IREs in the 5′-UTR (44, 45).

A modified IRE was predicted previously to be present in the coding region of APP mRNA at a site immediately upstream of the Aβ peptide domain in the APP ectodomain (46). Tanzi and Hyman (46) suggested that familial Alzheimer's disease mutations might disrupt stem loop formation to generate disease-associated phenotypes (46). However, clinically silent mutations for AD were also shown to disrupt the IRE secondary structure (47) leaving the physiological significance of the stem loop uncertain. Our data lend weight to a model for IRP binding to APP mRNA at an upstream site in the 5′-UTR of APP mRNA consistent with the responsiveness of these sequences to iron. We are further investigating the physiological relevance of the IRE in the Aβ peptide region of APP mRNA in concert with this upstream IRE-Type II.

The data in this report point to the presence of an iron-regulatory domain in the APP mRNA 5′-UTR that is absent in the APLP-1 mRNA. The alignments in Figs. 2 and 7 show that APP 5′-UTR sequences are selectively homologous with the ferritin mRNA IRE in two restricted homology clusters (+51 to +66) and (+82 to +94), which is absent from the corresponding APLP-1 5′-UTR sequence (Figs. 2 and 7). Wasco *et al.* (48) showed that APLP-1 and APLP-2 are homologous proteins to APP. Knock-out mouse studies confirmed their functional redundancy, because APP and APLP-1 APLP-1/APP knock-outs are viable (APLP-2/APP double knock-outs are lethal (49)). Therefore the iron-regulatory domain in the APP 5′-UTR appears unique to the Aβ precursor relative to APLP-1 and APLP-2. It remains to be determined whether the APP 5′-UTR is both a copper- and iron-regulatory element. Alternatively the APP 5′-UTR may operate selectively in response to iron, and APLP-1 and APLP-2 may be more responsive to different metals (*i.e.* copper and zinc).

Our finding that steady-state levels of intracellular APP are tightly regulated by iron is consistent with the preliminary clinical studies showing that copper and iron chelation may therapeutically reduce APP levels and lower Aβ peptide product in brain subregions. Inhibition of APP translation mediated through the APP 5′-UTR provides another mechanism by which chelators could be therapeutic agents for the treatment of AD patients (35, 50).

Acknowledgements—We are endebted to Dr. Dominic Walsh, Dr. Lars Nilsson, Dr. Frank Bunn, Dr. Kenneth Bridges, Dr. Huntington Potter, and Dr. Dennis Selkoe for continued support. Dr. Howard Fillit and Dr. Lorenzo Refolo have provided helpful support and discussion. We are particularly grateful to Nathan Best for assistance with the graphics and Sandra Payton and Amanda Venti for providing technical support.

REFERENCES

1. Selkoe, D. J. (1996) *J. Biol. Chem.* **271,** 18295–18298
2. Mucke, L., Masliah, E., Yu, G. Q., Mallory, M., Rockenstein, E. M., Tatsuno, G., Hu, K., Kholodenko, D., Johnson-Wood, K., and McConlogue, L. (2000) *J. Neurosci.* **20,** 4050–4058
3. Multhaup, G., Schlicksupp, A., Hesse, L., Beher, D., Ruppert, T., Masters, C., and Beyreuther, K. (1996) *Science* **271,** 1406–1409
4. Bush, A., Pettingell, W. H., Multhaup, G., Paradis, D., Vonsattel, J. P., Gusella, J. F., Beyreuther, K., Masters, C. L., and Tanzi, R. E. (1994) *Science* **265**, 1464–1467
5. Tanzi, R. E., Gusella, J. F., Watkins, P. C., Bruns, G. A., St George-Hyslop, P., Van Keuren, M. L., Patterson, D., Pagan, S., Kurnit, D. M., and Neve, R. L. (1987) *Science* **235,** 880–884
6. Kang, J., Lemaire, H. G., Unterbeck, A., Salbaum, J. M., Masters, C. L., Grzeschik, K. H., Multhaup, G., Beyreuther, K., and Muller-Hill, B. (1987) *Nature* **325,** 733–736
7. Saitoh, T., Sundsmo, M., Roch, J. M., Kimura, N., Cole, G., Schubert, D., Oltersdorf, T., and Schenk, D. B. (1989) *Cell* **58,** 615–622
8. van Leeuwen, F., de Kleijn, D. P. V., van den Hurk, H. H., Neubauer, A., Sonnemans, M. A. F., Sluijs, J. A., Koycu, S., Ramdjielal, R. D. J., Salehi, A., Martens, G. J. M., Grosveld, F. G., Burbach, P. H., and Hol, E. M. (1998) *Science* **279**, 242–247
9. Rogers, J. T., Leiter, L. M., McPhee, J., Cahill, C. M., Zhan, S. S., Potter, H., and Nilsson, L. N. (1999) *J. Biol. Chem.* **274,** 6421–6431
10. Komori, N., Kittel, A., Kang, D., Shackelford, D., Masliah, E., Zivin, J. A., and Saitoh, T. (1997) *Brain Res. Mol. Brain Res.* **49,** 103–112
11. Mbella, E. G., Bertrand, S., Huez, G., and Octave, J. N. (2000) *Mol. Cell. Biol.* **20,** 4572–4579
12. Eisenstein, R., and Theil, E. (2000) *J. Biol. Chem.* **275,** 40659–40662
13. Theil, E. (1987) *Ann. Rev. Biochem.* **56,** 289–315
14. Rogers, J. (1992) (Lauffer R, ed), pp. 77–104, CRC Press, Inc., Boca Raton, FL
15. Rogers, J. T., and Munro, H. N. (1987) *Proc. Natl. Acad. Sci. U. S. A.* **84,** 2277–2281

16. Thomson, A. M., Rogers, J. T., and Leedman, P. J. (2000) *J. Biol. Chem.* **275,** 31609–31615
17. Schalinske, K., Blemings, K., Steffen, D. W., Chen, O. S., and Eisenstein, R. S. (1997) *Proc. Natl. Acad. Sci. U. S. A.* ***94***, 10681–10686
18. LaVaute, T., Smith, S., Cooperman, S., Iwai, K., Land, W., Meyron-Holtz, E., Drake, S. K., Miller, G., Abu-Asab, M., Tsokos, M., Switzer, R., Grinberg, A., Love, P., Tresser, N., and Rouault, T. A. (2001) *Nat. Genet.* **27,** 209–214
19. Kim, H.-Y., Klausner, R. D., and Rouault, T. A. (1994) *J. Biol. Chem.* **270**, 4983–4986
20. Thomson, A. M., Rogers, J. T., and Leedman, P. J. (1999) *Int. J. Biochem. Cell Biol.* **31,** 1139–1152
21. Leedman, P., Stein, A. R., Chin, W. W., and Rogers, J. T. (1996) *J. Biol. Chem.* **271**, 12017–12023
22. Iwai, K., Drake, S. K., Wehr, N. B., Weissman, A. M., LaVaute, T., Minato, N., Klausner, R. D., Levine, R. L., and Rouault, T. A. (1998) *Proc. Natl. Acad. Sci. U. S. A.* **95,** 4924–4928
23. Sampietro, M., Caputo, L., Casatta, A., Meregalli, M., Pellagatti, A., Tagliabue, J., Annoni, G., and Vergani, C. (2001) *Neurobiol. Aging* **22,** 563–568
24. Bartzokis, G., Sultzer, D., Cummings, J., Holt, L. E., Hance, D. B., Henderson, V. W., and Mintz, J. (2000) *Arch. Gen. Psychiatry* **57,** 47–53
25. Lovell, M. A., Robertson, J. D., Teesdale, W. J., Campbell, J. L., and Markesbery, W. R. (1998) *J. Neurol. Sci.* **158,** 47–52
26. Connor, J. R., Boeshore, K. L., Benkovic, S. A., and Menzies, S. L. (1994) *J. Neurosci. Res.* **37,** 461–465
27. Pinero, D. J., Hu, J., and Connor, J. R. (2000) *Cell. Mol. Biol.* (*Noisy-le-grand*) **46,** 761–776
28. Robinson, S., Noone, D. F., Kril, J., and Haliday, G. M. (1995) *Alzheimer's Res.* **1**, 191–193
29. Bodovitz, S., Falduto, M. T., Frail, D. E., and Klein, W. L. (1995) *J. Neurochem.* **64**, 307–315
30. Buxbaum, J. D., Choi, E. K., Luo, Y., Lilliehook, C., Crowley, A. C., Merriam, D. E., and Wasco, W. (1998) *Nat. Med.* **4,** 1177–1181
31. Buxbaum, J., Oishi, M., Chen, H. I., Pinkas-Kramarski, R., Jaffe, E. A., Gandy, S. E., and Geengard, P. (1992) *Proc. Natl. Acad. Sci. U. S. A.* **89**, 10075–10078
32. Mullner, E., Neupert, B., and Kuhn, L. C. (1989) *Cell* **58,** 373–382
33. Thomson, A. M., Rogers, J. T., Walker, C., E., Staton, J. M., and Leedman, P. J. (1999) *Biotechniques* **27,** 1032–1039
34. Selkoe, D. J., Berman Polisny, M., Joachim, C. L., Vickers, E. A., Lee, G., Fritz, L. C., and Oltersdorf, T. (1988) *Proc. Natl. Acad. Sci. U. S. A.*, **85,** 7341–7345
35. Cherny, R., Atwood, C. S., Xilinas, M. E., Gray, D. N., Jones, W. D., McLean, C. A., Barnham, K. J., Volitakis, I., Fraser, F. W., Kim, Y., Huang, X., Goldstein, L. E., Moir, R. D., Lim, J. T., Beyreuther, K., Zheng, H., Tanzi, R. E., Masters, C. L., and Bush A. I. (2001) *Neuron* **30**, 641–642
36. Rogers, J. T. (1996) *Blood* **87,** 2525–2537
37. Zuker, M. (1989) *Science* **244,** 48–52
38. Eckblom, J. (2001) *Drug Discov. Today* **6,** 1259–1260
39. Toth, I., Yuan, L., Rogers, J. T., Boyce, H., and Bridges, K. R (1999) *J. Biol. Chem.* **274,** 4467–4473
40. Gray, N., Quick, S., Goossen, B., Constable, A., Hirling, H., Kuhn, L. C., and Hentze, M. (1993) *Eur. J. Biochem.* **218,** 657–667
41. Cox, L. A., and Adrian, G. S. (1993) *Biochemistry* **32,** 4738–4745
42. Feng, Y., Zhang, F., Lokey, L. K., Chastain, J. L., Lakkis, L., Eberhart, D., and Warren, S. T. (1995) *Science* **268,** 731–734
43. Cox, T. C., Bawden, M. J., Martin, A., and May, B. K. (1991) *EMBO J.* **10,** 1891–1902
44. Donovan, A., Brownlie, A., Zhou, Y., Shepard, J., Pratt, S. J., Moynihan, J., Paw, B. H., Drejer, A., Barut, B., Zapata, A., Law, T. C., Brugnara, C., Lux, S. E., Pinkus, G. S., Pinkus, J. L., Kingsley, P. D., Palis, J., Fleming, M. D., Andrews, N. C., and Zon, L. I. (2000) *Nature* **403,** 776–781
45. McKie, A. T., Marciani, P., Rolfs, A., Brennan, K., Wehr, K., Barrow, D., Miret, S., Bomford, A., Peters, T. J., Farzaneh, F., Hediger, M. A., Hentze, M. W., and Simpson, R. J. (2000) *Mol. Cell* **5,** 299–309
46. Tanzi, R. E., and Hyman, B. T. (1991) *Nature* **350,** 564
47. Zubenko, G., Farr, J., Stiffler, S., Hughes, H. B., and Kaplan, B. B. (1992) *J. Neuropathol. Exp. Neurol.* **51**, 459–463
48. Wasco, W., Gurubhagavatula, S., Paradis, M. D., Romano, D. M., Sisodia, S. S., Hyman, B. T., Neve, R. L., and Tanzi, R. E. (1993) *Nat. Genet.* **5,** 95–100
49. von Koch, C. S., Zheng, H., Chen, H., Trumbauer, M., Thinakaran, G., van der Ploeg, L. H., Price, D. L., and Sisodia, S. S. (1997) *Neurobiol. Aging* **18,** 661–669
50. Crapper McLachlan, D., Dalton, A. J., Kruck, T. P. A., Bell, M. Y., Smith, W. L., Kalow, W., and Andrews, D. F. (1991) *Lancet* **337**, 1304–1308

An Iron-responsive Element Type II in the 5′-Untranslated Region of the Alzheimer's Amyloid Precursor Protein Transcript

Jack T. Rogers, Jeffrey D. Randall, Catherine M. Cahill, Paul S. Eder, Xudong Huang, Hiromi Gunshin, Lorene Leiter, Jay McPhee, Satinder S. Sarang, Tada Utsuki, Nigel H. Greig, Debomoy K. Lahiri, Rudolph E. Tanzi, Ashley I. Bush, Tony Giordano and Steve R. Gullans

J. Biol. Chem. 2002, 277:45518-45528.
doi: 10.1074/jbc.M207435200 originally published online August 26, 2002
